Standing on the shoulder of a giant landslide: an InSAR look at a slow-moving hillslope under melting glaciers in the western Karakoram

Said Mukhtar Ahmad[1,2], Nitheshnirmal Sadhasivam[1], Mona Lisa[2], Luigi Lombardo[1], Mustafa Kemal Emil[3], Islam Fadel[2], Cees J. Van Westen[1], Amira Ahmed[1], Hakan Tanyaş[1*]

[1]University of Twente, Faculty of Geo-Information Science and Earth Observation (ITC), Enschede, Netherlands[2]

[2]Department of Earth Sciences, Quaid i Azam University Islamabad, Pakistan

[3]Geological and Environmental Sciences Department, Western Michigan University, Kalamazoo, USA

*Corresponding author: Hakan Tanyaş (h.tanyas@utwente.nl)

Abstract

Understanding the cascading effects of glacier melting in terms of large slope deformation in high mountainous areas could come from the use of Interferometric Synthetic Aperture Radar (InSAR) techniques. In this work, we investigate a slow moving, extremely large landslide (~20 km^2) in the Chitral region in Northern Pakistan, which threatens several villages. Our InSAR analyses, using Sentinel-1 data which span a period of six years, allowed us to retrieve the spatio-temporal pattern of downslope deformation for both ascending and descending orbits. The results highlight a worrying situation where the crown of the landslide is moving relatively fast (from 36 to 80 mm/yr). Several sackung-type of movements and other signs of instability were observed in many locations over the crown. As for the toe of the large landslide, a western sliding sector offers a different mechanism than its eastern counterpart where the deformation appears to accumulate through time. This brief description has two implications. One from the most practical perspective, as it calls for further studies and attention from local administrations. And, it also scientifically highlights the strength of InSAR when it comes to unveiling slow deformation regimes, which may be invisible through the eye of other techniques, although they may still lead to catastrophic failures. Such considerations can be even framed beyond the scale explored in this manuscript. In ither words, the same mechanism and threat to local communities can be present across the whole Hindukush-Himalayan-Karakoram range, where glaciers are widely receding due to climate change.

Keywords: InSAR; slow-moving landslide; climate change; snowmelt

1. Introduction

The genesis of landslides in mountainous terrains is strongly associated with climatic factors (Stoffel and Huggel, 2012) such as variations in temperature, rainfall intensity and/or snowmelt, which are expected to worsen in the future due to climate change (Beniston et al., 2018; Gobiet et al., 2014). Since late 1900, reports of widespread and increasingly frequent slope failures in high portions of the Alps (Huggel et al., 2012; Stoffel et al., 2014) have brought attention to the effects of climate change on the dynamics of slope failures. Recent studies have also pointed at the effects of climate change in the future (Gobiet and Kotlarski, 2020; Ikeda et al., 2021; IPCC, 2021). Under many climate change scenarios, climatic extremes are likely to increase the magnitude and frequency of landslide events in mountainous terrain (Gruber and Haeberli, 2007; Seneviratne et al., 2012). Moreover, the threat they may pose to mountainous communities may become even more severe in the years to come (Gariano and Guzzetti, 2016; Stoffel et al., 2014).

The evidence collected by the geoscientific community in the last several decades indicates an increasing warming rates specifically at higher elevations in some regions (Pepin et al., 2022) and retrieving of glaciers almost everywhere around the globe (Ashish et al., 2006; Huss and Hock, 2018; Zemp et al., 2019). Specifically, shrinking of glaciers have been reported across all latitudes, from artic or peri-artic mountain belts including Alaska, western North America and British Columbia (Hewitt et al., 2008), to Asian and the Hindukush-Himalayan-Karakoram (HHK) mountain ranges (Bolch et al., 2019; Bräuning, 2006). The retreat of most glaciers across the HHK mountain ranges took place faster than any other glaciers. It was related to the local increase in surface air temperature (IPCC, 2021). Prasad et al. (2009) add more details to this description, pointing at the widespread receding behavior of glaciers and snow cover over the Himalayan region.

Given the significant influences of global warming, the HHK mountain range offers a unique opportunity to explore the link between climate change and landsliding. Among various climatic factors, the slope equilibrium is particularly sensitive to variations in precipitation and temperature regimes as they can alter pore pressure of hillslope materials (Loche et al., 2022). Generally, rapid increase in water content leads to changes in pore water pressure and slope stability (Al-Umar et al., 2020; Gariano and Guzzetti, 2016), which in high-mountain environments can be worsened by the thawing of permafrost and snow cover (Osawa et al., 2017). As a result, these processes may disturb hillslope stability (Marcer et al., 2021). This is the case reported in a Swiss site in 1999 (Eberhardt et al., 2005) when the combined action of snow melting and heavy rain contributed to the initiation of more than 350 landslides and debris flows. The same phenomenon has been attributed to landslides that periodically occur in Hokkaido (Japan) at the start of the snow-melting season, from April to May (Ishikawa et al., 2015).

Among various mountain ranges, the HHK belt (Fig. 1) constitutes a region of particular geomorphological relevance in terms of landsliding. The rugged topography, combined with extreme climatic events (Riaz et al., 2019), strong seismicity (Ray et al., 2009; Shafique et al., 2016) and anthropogenic influence (Rahman et al., 2014) result in a unique landscape prone to landslides. This is also confirmed in terms of raw numbers, as 30% of the world's landslides occur in this region (Atta-ur-Rahman et al., 2011).

The Karakoram Himalayan region, including northern Pakistan host many rock avalanches and debris slides, which repeatedly occurring over thousands of years or more, while threatening local settlements (Hewitt et al., 2008). Some of the largest slope failures (i.e., with planimetric area between 2 km^2 and 55 km^2) occurred along the Kohistan Ladakh arc (Hewitt, 2001) as well as in the Hunza and Gilgit valleys of the Karakoram (Gao et al., 2021) region, being associated with climatic stresses. For instance, the well-known Attabad rockslide (1200 m long, 350 m wide and 125 m high) occurred on January 4, 2010 during the rainy season and blocked the Hunza river, forming the current Gojal lake (Kargel et al., 2010). It caused 19 victims and the displacement of 1650 people (Cook and Butz, 2013).

For the HHK, the relation between landslide occurrence and variation in temperature patterns due to climate change and the resulting permafrost/snow melt are yet to be explored in depth. The reason behind this literature gap is mainly due to the lack of long-term hillslope monitoring records. This is not surprising as logistics across the north Pakistan range can be prohibitive if not impossible at specific locations.

The birth and spread of Interferometric Synthetic Aperture Radar (InSAR) has set the stage to address such problems and retrieve detailed records of slow surface deformation in space and time (Casagli et al., 2010; Cascini et al., 2010; Colesanti and Wasowski, 2006; Hilley et al., 2004; Schlögel et al., 2015). This technique has gained the spotlight over the years with the launch Sentinel-1 mission because of its global coverage, applicability over wide areas and detailed information provided both in space and time (e.g., Mondini et al., 2021; Wasowski and Bovenga, 2014). Among the most renowned applications, land subsidence and landslide monitoring have demonstrated the importance of the InSAR technique in geomorphological applications (e.g., Samsonov et al., 2020; Sato and Une, 2016). The latter case has mainly focused on slow-moving landslides (Bayer et al., 2018; Lacroix et al., 2020; Schlögel et al., 2015; Wasowski and Pisano, 2020) and in some cases, to identify them over large areas (Bekaert et al., 2020; Liu et al., 2021; Xu et al., 2021). Among the available InSAR techniques, Persistent Scatterer Interferometry (PSI) and Small Baseline interferometry (SBAS) have been further developed over the years and employed to measure ground motion for various applications (e.g., Hungr et al., 2001; Tantianuparp et al., 2013). As a result, millimeter-accuracy deformation measurements can be nowadays estimated globally and in many terrain conditions (e.g., Perissin and Wang, 2011). Notably, PSI extends this framework by deriving time series of deformation measurements. Specifically, this is achieved by using a stack of SAR images of the same area, repeatedly collected to estimate the displacement and velocity of the earth's surface using the differences in the SAR signal (e.g., Huang Lin et al., 2019).

However, few studies have incorporated InSAR-based analyses to examine landslide evolution processes across the north of Pakistan/western Karakoram terrain. Hussain et al., (2021) apply InSAR-based analyses to Chitral region but the research focuses on generating a landslide susceptibility map for the area and lacks the information regarding slow-moving landslides or the investigation of possible failures governed by permafrost or snow melt. In fact, even the presence of permafrost in the HHK has hardly been investigated (Gruber et al., 2017). Rehman et al. (2020) identify some slow-moving landslides in the western Karakoram using InSAR and examine the possible role of precipitation and seismic events.

Notably, the limited literature implies that we still lack information regarding slow-moving landslides, their causes and possibly threatened settlements in the northern Pakistan/western Karakoram terrain. Our objective is to add to this literature and explore the use of InSAR deformation data to monitor a large, slow-moving landslide in the region; under the assumption that at least part of the deformation may be induced by climate change effects.

We specifically focus on a possible hazardous area highlighted by Stauffer (1975) half a century ago but not subjected to further study. In a report of the U.S. Geological Survey, Stauffer (1975) described several dangerous slow-moving landslides across the Chitral sector. The report particularly mentions a large, slow-moving landslide body, most likely formed due to "not a single rapid event" but a continuous deformation process lasting many years north of the Reshun village (Fig. 1b). Stauffer (1975) also reports many small and large landslides taking place on top of this slow-moving large body from time to time, are mobilized after heavy rains.

Therefore, by targeting this area, our study addresses two needs. On the one hand and from a more theoretical standpoint, we aim at exploring the mechanism of this slow-moving landslide in western Karakoram to improve our understanding of the link between landslides and mainly climatic factors. On the other hand, and more practically, we also aim to assess the threat posed by this large, slow-moving landslide over the nearby villages of Loan and Reshun.

2. Study area

Our study area is located in the Hindukush-Karakoram mountain range proximal to the Loan and Reshun Villages in Chitral, NW of Pakistan (Fig. 1). Chitral lies along the north west boundary of Pakistan and comprises rugged terrains with high elevated peaks that can reach altitudes up to 7000 m (Fig. 2). As a result, most of our study area is overlooked by mountains that are covered in snow all over the year.

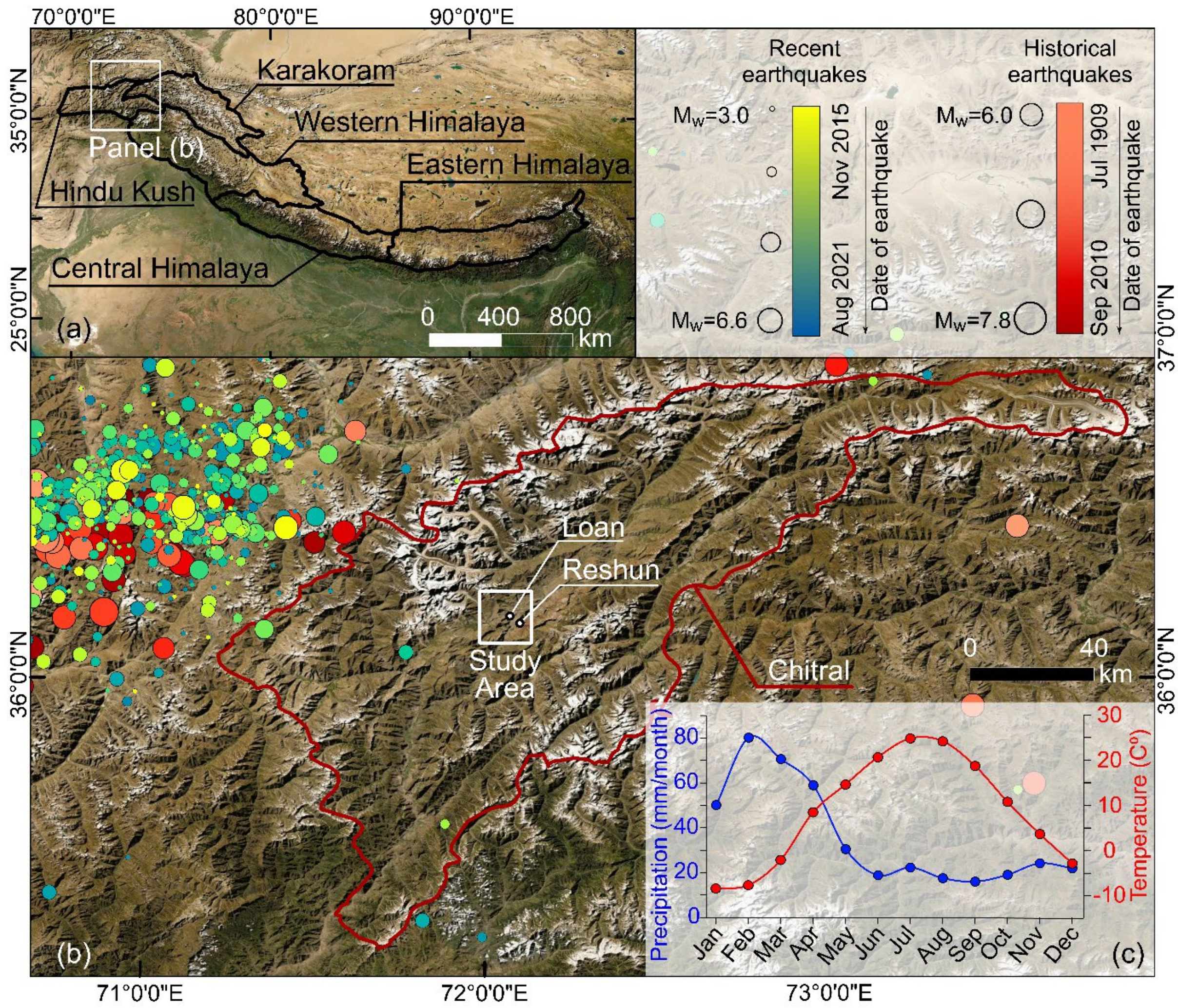

Figure 1. Panels showing location map of Chitral (a) and the study area overlaid by epicenters of historical earthquakes (b, USGS, 2021) as well as monthly average precipitation amounts of the study area indicated by the white rectangle in panel (c). The average precipitation values were calculated based on the 20-year time series of IMERG Final Run product (Huffman et al., 2019).

Overall, the Chitral region does not host strong earthquakes historically. Actually, no earthquakes of magnitude greater than 6.0 have been recorded within the Chitral region in the last century (USGS, 2021; Fig. 1b). Nevertheless, a number of large earthquakes were have occurred in a zone between 50-100 km from the study area. The closest ones occurred on 4th January 2019 (M_w=4.5 and depth= 113 km) and (M_w=4.1 and depth= 107 km) at 30 km and 45 km far from our study area, respectively.

Based on the 20 years (between 2000 and 2020) time series of FLDAS Noah Land Surface Model (McNally, 2018) and the Integrated Multi-Satellite Retrievals (IMERG) Final Run product (Huffman et al., 2019) large variations in both temperature and precipitaion have been measured in the study area. The area experiences warm summers and cold winters, with maximum and minimum average temperatures between -10° and 25° (Fig. 1c). The period between January and April appears as the wettest season in the area, where monthly average rainfall changes from 50 to 80 mm (Fig. 1c).

Three main geological structures run with a NE-SW direction across the Chitral sector namely, the Reshun fault, the Tirich Mir fault (Fig. 2) and the Main Karakoram suture zone (Coward et al., 1986; Zanchi and Gaetani, 2011). These three faults marked the collision of three micro plates from the Jurassic to the Cretaceous (Gaetani et al., 1996; Zanchi et al., 1997). During the last episode of the Himalayan orogeny, Karakoram and southern Hindukush underwent a series of tectonic deformations including a marked uplifting (Heuberger et al., 2007). This compressive regime has been recorded in the main lithological formations outcropping within our study area. Specifically, four geological units can be found, consisting of carbonates and quarzitic rocks (Shogram Formation, Devonian), overlain by carbonate rocks of high metamorphosed grade (Reshun marble, Cretaceous) further underlaying shales (Loan unit, Devonian-Carboniferous) and slates and phyllite (Wakhan unit Devonian). For further information on the geological and tectonic context, we refer to Tahirkheli et al. (2012) and Sarwar and Rahman (2016).

Several researchers in the HHK region pointed out the strong lithological control on the failure mechanism. Gerrard (1994) refers to landslide kinematics related to specific structural features, rock types and regolith. Gullà et al. (2004) add further comments on this, stressing the role of deep weathering, responsible for the alteration of mineralogy along preferential directions, which set the stage for the failure to take place. In particular, shale and schists are susceptible to translational sliding whereas slopes that host phyllites mainly give rise to rockfalls, in contrast to quartzite lithotypes that generally do not present slope instabilities (Gerrard, 1994). Due to these considerations, we recognize the villages within our study area to be potentially under threat as shales widely outcrop (Fig. 2).

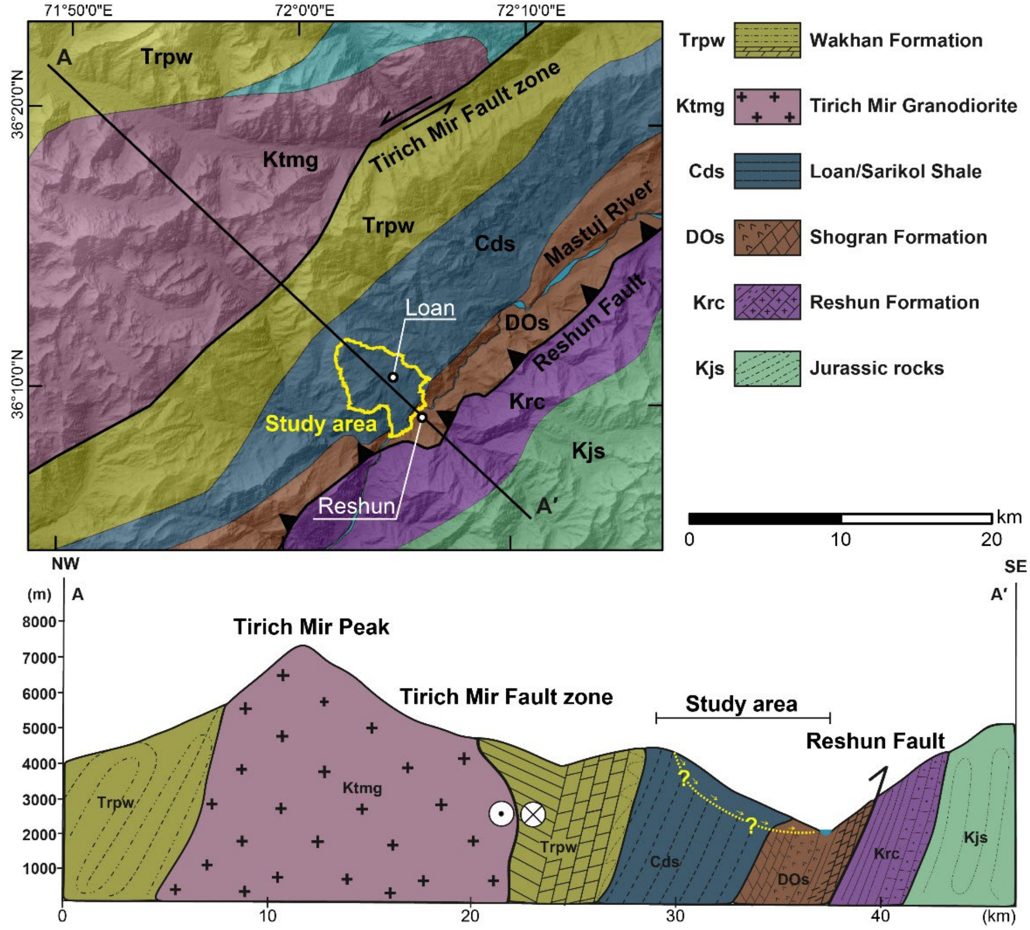

Figure 2. Geological map and cross section of the study area.

Morphotectonically, while examining the area indicated by Stauffer (1975) from satellite images (Fig. 3), we recognized a number of features hosted in an old and extremely large (15.7 km^2) landslide mass (see black polygon in Fig. 3a). This landslide likely mobilized as a result of the failure of a quartzite wedge acting as a barrier at the foothill of a large steeping slope (Fig. 3c). To confirm or reject this hypothesis, we conducted a visit to the site. The field observations confirmed the presence of a numerous evidences of slope deformation (see red polygon in Fig. 3a), such as numerous tension cracks on slopes with a sackung-like appearance (Figs. 3 and 4b-4d).

Sackung type of slope movements are common in high-relief and glaciated terrains (Zischinsky, 1968) and are characterized by prominent features such as uphill-facing scarps, trenches or depressions, tension cracks and toe bulging. They can involve large (i.e., >100 m) downslope displacements of rock at rates of a few millimeters to several meters per year (e.g., Dehn et al., 2000; Mccoll and Davies, 2013).

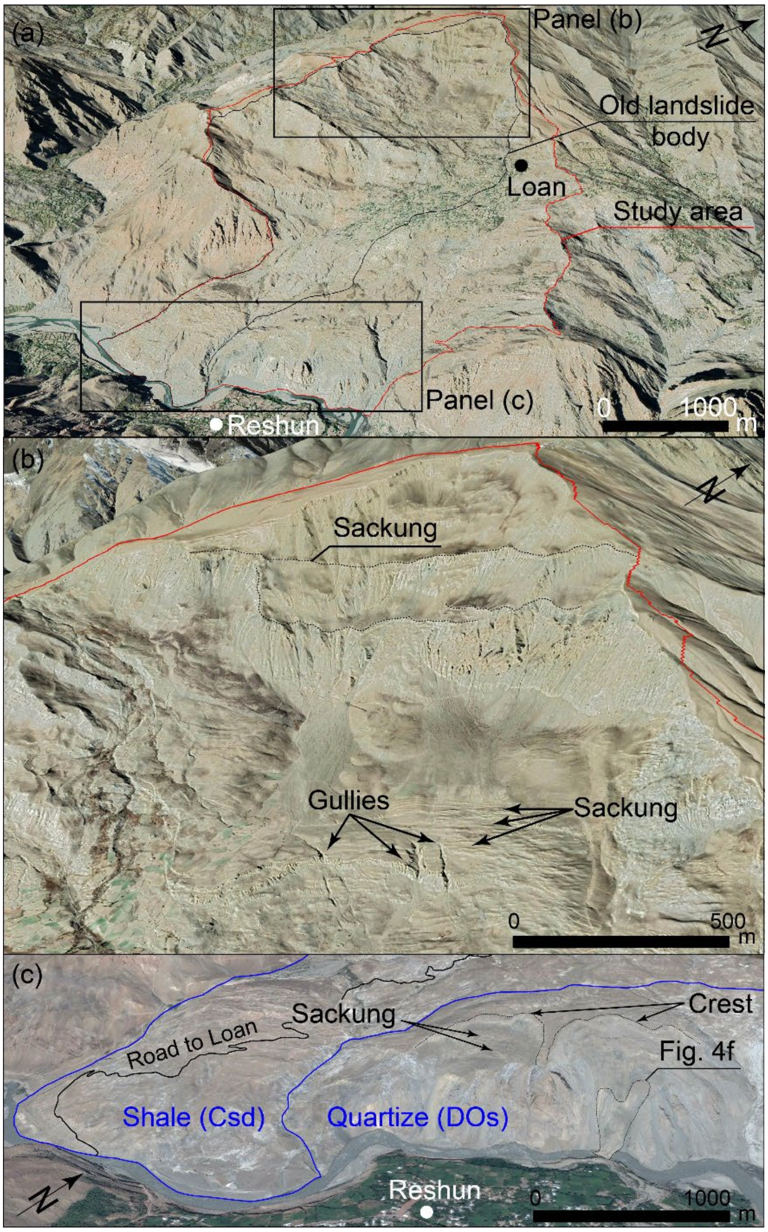

Figure 3. Various morphological features reflecting landscape deformations across the examined watershed.

In our study area, in a number of sites overlooking the village of Loan, we noted widespread signals of sackung features, these being the manifestation of a deep-seated and slow-moving landslide, which host debris avalanches and gullies (Fig. 3b). Moreover, tensional cracks were observed mostly at the foothills (Figs. 3 and 4). As another reflection of possible surface deformations unrevealed by a number of morphological features, damaged houses are also quite common in the Loan village (Fig. 4e). Local people we interviewed indicated that there is almost no building without any damage in the village.

Figure 4. Pictures showing (a) locations of various field observations reflecting (b-d) sackung features and tension cracks, (e) cracks in a house within the Loan village and (f) a rock avalanche occurred on 5th of March 2017.

Apart from slowly occurring surface deformations, flow type landslides and rock avalanches are also common, especially towards the lower section of the study area. Local people informed us that debris flows and rock avalanches frequently obstruct the road between the villages of Reshun and the Loan during spring time. In fact, on 5th of March 2017, our local contact from the Reshun village witnessed a rock avalanche (Fig. 4f), likely due to the combined action of snow melt and riverbank erosion from below.

3. Methodology and data

In this study, we used an InSAR time series analysis approach and two sets of Sentinel-1 data stacks collected in ascending and descending orbital geometries (Table 1) to quantify the dynamic behavior of slow-moving landslides in the western part of the Karakoram region. Among these orbits, the ascending one provides a side-view, whereas its descending counterpart scans the hillslope under examination, which is facing towards south-east, with almost a perpendicular angle to the slope face (Fig. 5).

Table 1. SAR data used in the analyses

Satellite	Sentinel-1 (SLC)	Sentinel-1 (SLC)
Orbit	Ascending	Descending
Beam	IW	IW
Path	173	5
Frame	111,112 and 113	471 and 472
Polarization	VV	VV
Heading angle (degree)	352	192
Incidence angle (mean±std. dev., degree)	42.2±2.4	33.0±14.5
Acquisition dates	Nov 2015-Aug 2021	Nov 2015-Aug 2021
Number of scenes	154	151

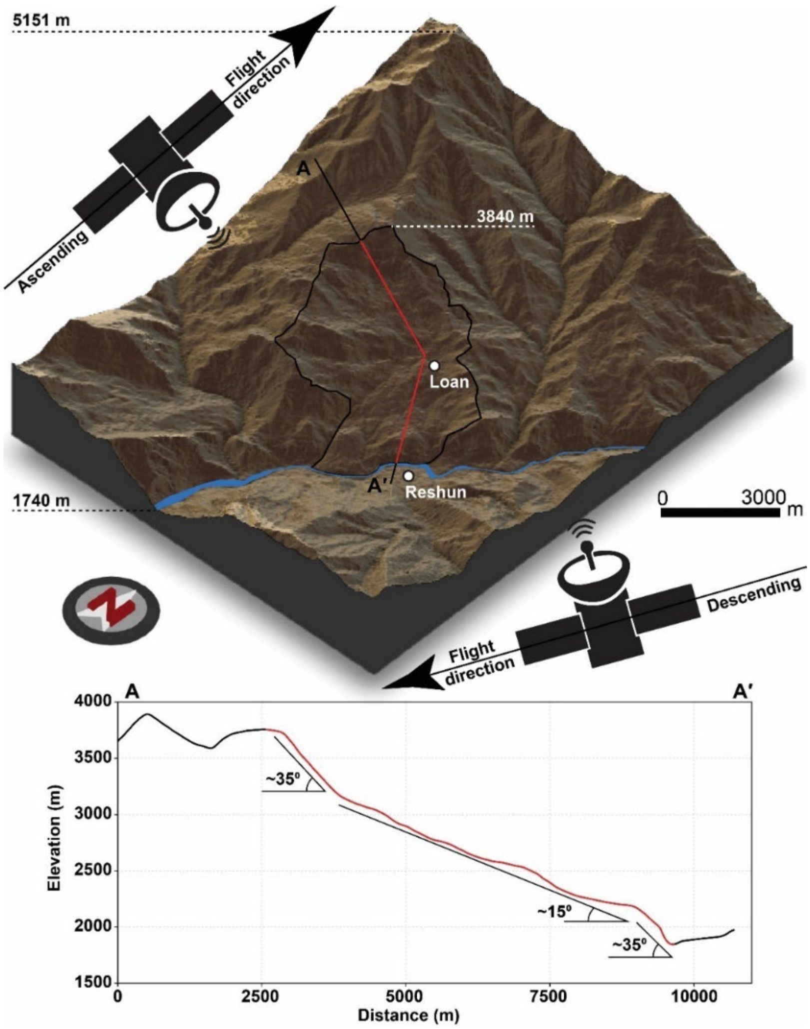

Figure 5. 3D elevation model of the study area showing ascending and descending Sentinel-1 orbits as well as topographic profile passing through the examined watershed.

These images have been collected from November 2015 to August 2021 and accessed through the Copernicus Open Access Hub of the European Space Agency. We obtained Sentinel-1 data in Single Look Complex (SLC) with interferometric-wide (I.W.) mode and vertical-vertical (V.V.) polarization (Table 1) and processed them in two phases, one in SNAP and one in Snap2Stamps, via the Stanford Method for Persistent Scatterer (StaMPS) (Hooper et al., 2012; Hooper, 2008). The StaMPS approach was used to perform the time-series analysis, whose overall summary is presented in the Supplementary Materials (see Fig. S1).

After generating Persistent Scatterer (PS) points providing line-of-sight (LOS) deformation time series and mean velocities, we converted them into their downslope components following the method described in the literature (Aslan et al., 2020; Notti et al., 2014). We made this conversation for both ascending and descending data separately. To identify active PS points, we examined summary statistics of average velocities and removed values smaller than one standard deviation (e.g., Aslan et al., 2020).

We also calculate the radar visibility index for the ascending and the descending Sentinel-1 orbits over the study area. We assess visibility through R-index (Cigna et al., 2014; Notti et al., 2014) to identify areas suffering from geometric distortions (i.e., foreshortening and layover).

We examine the spatial distribution of PS points and corresponding displacement velocity over aspect-wise homogenous landscape partitions called Slope Unit (SU) using the r.slopeunits software module (Alvioli et al., 2016). The use of SUs in slope stability assessments (Carrara, 1988) and landslide susceptibility/hazard studies (Lombardo et al., 2021; Tanyaş et al., 2019) has recently gained attention in the geomorphological community. The way we used an SU partition here is different from the data-driven context mentioned above. We aggregated the deformation signal of all PS points contained within a given SU. In other words, we translated the point-wise deformation velocity and deformation time series into mean deformation velocity and mean deformation time series associated with the whole portion of the slope profile, i.e., the SUs themselves.

We also used the Shuttle Radar Topography Mission (SRTM) digital elevation model, with 1 arc-second spatial resolution (NASA JPL, 2013) for various operations, including geocoding Sentinel-1 images, topographical phase removal, radar visibility analyses, conversion between LOS and downslope deformations and for the generation of SUs. To analyze surface deformation with respect to climatic variables, we generated time series for various climatic variables. Specifically, we used FLDAS Noah Land Surface Model, with 0.01° spatial and 1 day temporal resolution for the surface temperature and fraction of snow cover and CHIRPS data with 0.05° spatial (McNally, 2018) and 1 day temporal resolution for the precipitation (Funk et al., 2015). To carry out similar analyses with respect to seismicity, we used the earthquake catalog of the U.S. Geological Survey (USGS).

4. Results

We examined Sentinel-1 scenes for both ascending and descending orbits. Overall, both orbits provided a good visibility (i.e., R-index>0.5, Notti et al., 2014) for the hillslope under examination (Figs. 6a and 6b). The area affected by geometric distortions are less than 5% in both cases.

To further assess the spatial distribution of PS points, we used a SU partition of the whole slope and calculated the density of PS points within each polygon. Results show that the PS point density is high in some SUs, reaching up to 680 PS per km^2. However, especially in SUs located in the highest portions of the topographic profile, the PS density appears low (~10 km^{-2}). Given the vegetation-free landscape of our study area (see Fig. 3), seasonal snow cover likely caused coherence loss and thus, low PS point density (e.g., Carlà et al., 2019).

Because of the large difference in the visibility, we opted to keep analyzing PS points generated from ascending and descending orbits separately. Our rationale is that some deformation signals could be captured only through one of the two orbits and therefore, separate analyses might enrich our overall understanding of the surface dynamics in the site.

The PS points located within the landslide zone showed larger LOS velocities compared to the surrounding slopes (Figs. 6c and 6d). In the ascending orbit, we captured mostly deformations away from the satellite (i.e., negative displacements), as one can expect based on the relative orientation of the hillslope (mostly facing East and Southeast) with respect to eastward looking geometry of Sentinel-1 ascending acquisitions. The maximum LOS velocity was -57 mm/year, thus we saturated values higher than -50 mm/year for a clearer visualization. As for the descending orbit, we identified mainly displacements towards the satellite, which is also expected given the dominant hillslope orientation with respect to westward looking geometry of the descending acquisition. In this case, the maximum LOS velocity was 51 mm/year, which we again visually saturated at 50 mm/year for consistency (Figs. 6c and 6d).

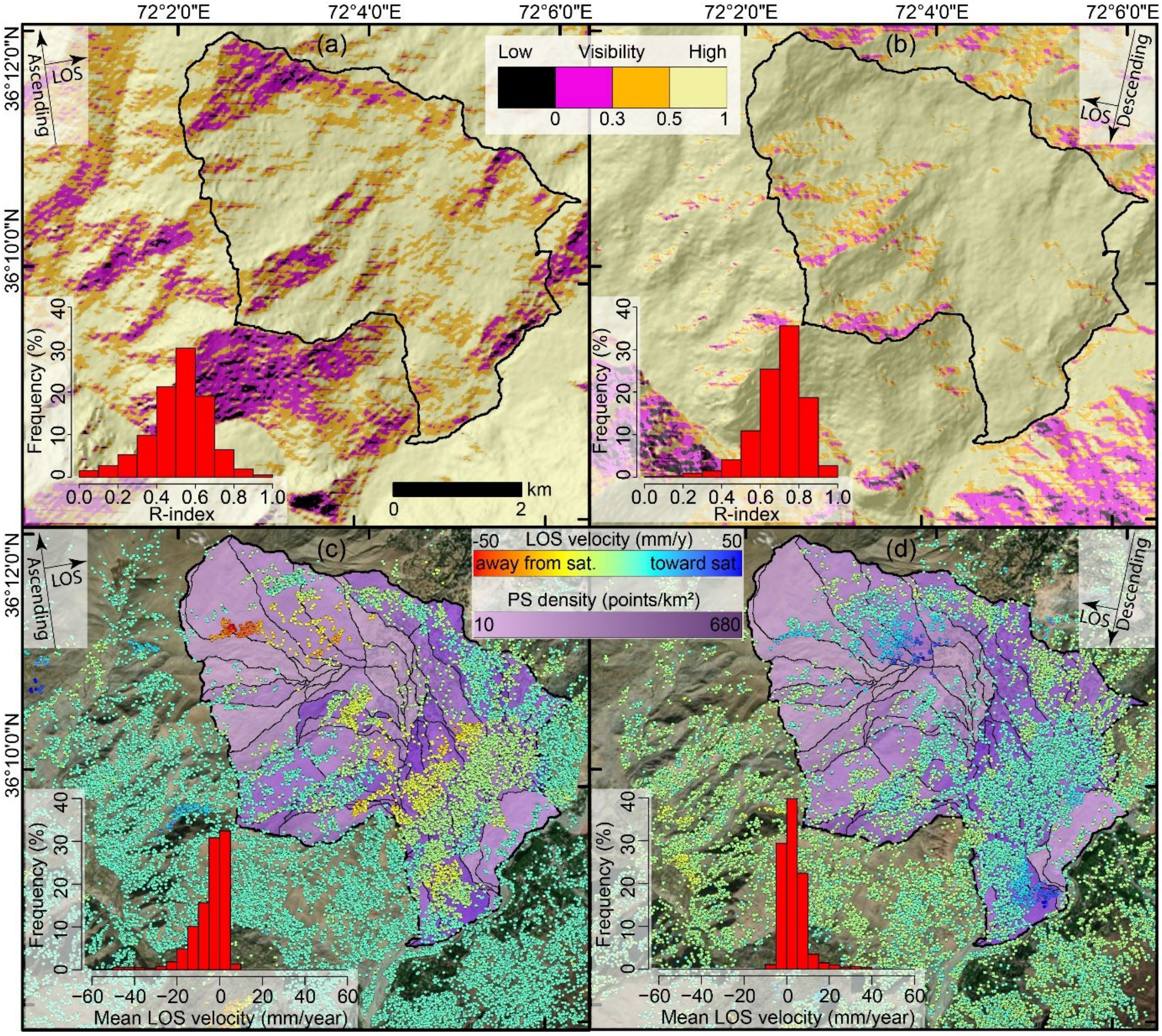

Figure 6. Panels showing (a-b) radar visibility (i.e., R-index) and (c-d) LOS mean velocity maps overlaid by PS densities for ascending and descending orbits, respectively. In all panels histograms are generated for the PS points located within the study area indicated by the black polygon.

To better assess possible hillslope deformations, we reprojected LOS mean velocities and corresponding deformation time series along the downslope direction (Fig. 7). The result of this conversion also revealed a similar spatial pattern highlighting areas with relatively large deformations (Fig. 7). Notably, downslope velocities are larger than their LOS counterparts. The downslope velocities vary between -170 mm/year to 164 mm/year for ascending and descending orbits, respectively. Even in this case we applied a saturation when converting this information into maps, not only to improve visibility but also because values outside the interval of -100 and 100 mm/year can be mostly considered outliers (Fig. 7).

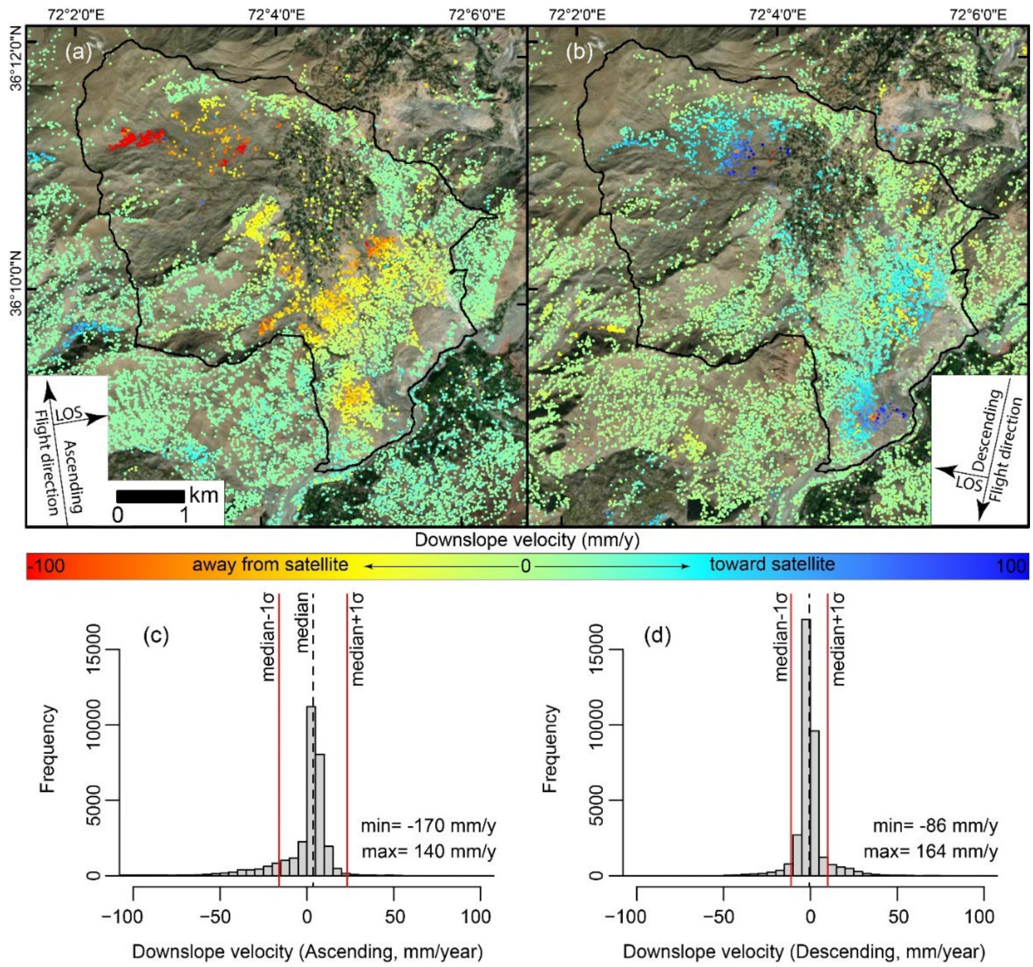

Figure 7. Downslope velocities (a-b) and their frequency distribution with median and standard deviation values (c-d) for ascending and descending orbits, respectively.

To identify actively deformed subsets of the hillslope, extreme values and their spatial distribution are more insightful than small values that could be considered as background level of deformation (e.g., Aslan et al., 2020). Therefore, to differentiate actively deformed areas, we filtered out those values between the median velocity and one standard deviation (±1σ). For the remaining PS points, we calculated average downslope velocities at the SU level in both ascending and descending orbits (Fig. 8). For the visualization of varying downslope velocities across the study area, we coupled the average velocities with the dominant slope direction of each SU. As a result, we clearly show that almost the entire area under consideration (~20 km^2) slowly moves downslope, except for a few SUs mainly located at the edges of the watershed (Fig. 8). The average downslope velocities aggregated at the finer SU scale (Figs. 8a and 8b) exhibit a substantial range of variation, from 10 to 130 mm/year. This implies that over the six-year time-window that our stack of SAR images covers, the maximum total deformations could locally reach up to 80 cm.

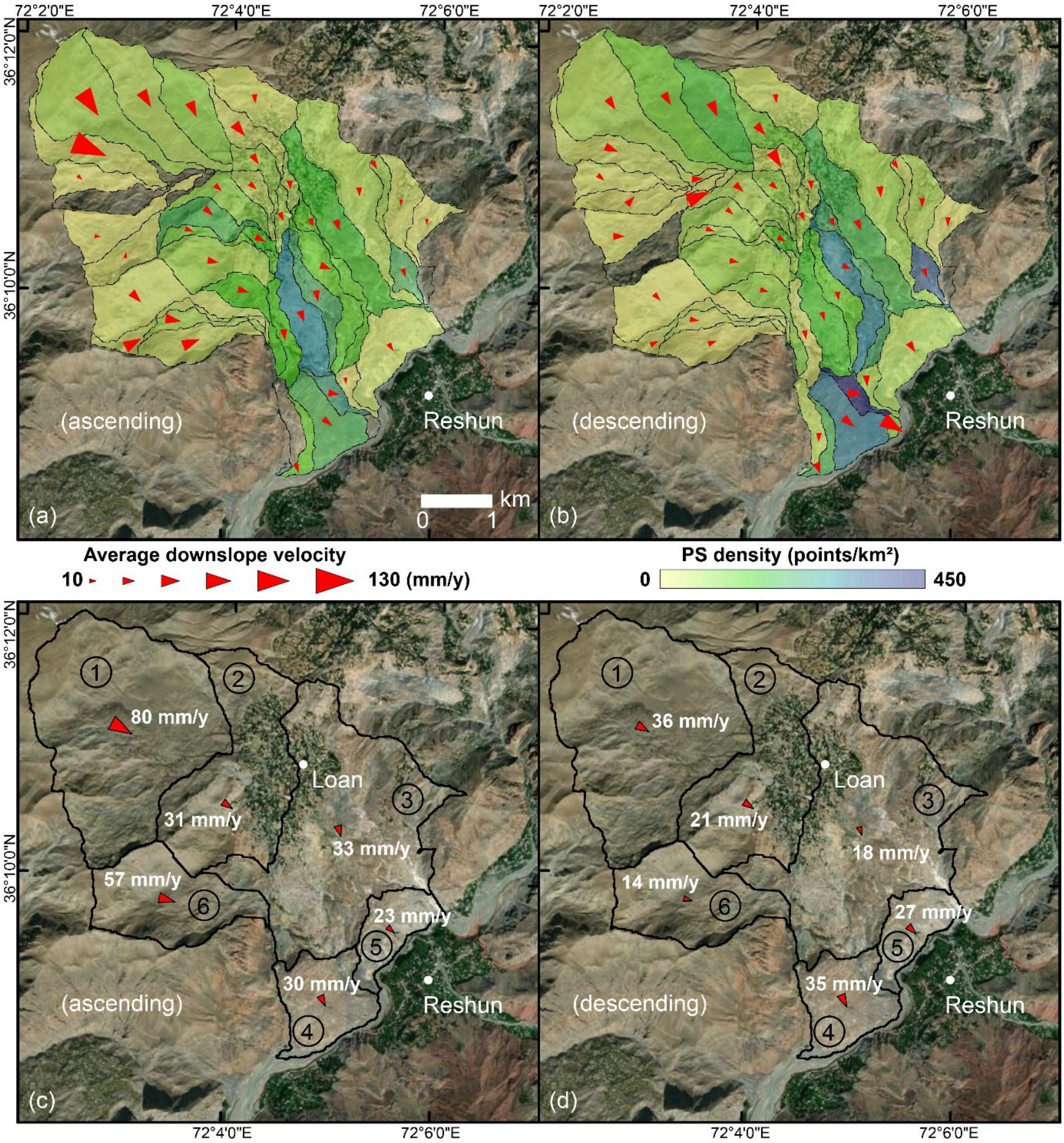

Figure 8. Downslope velocities overlaid by PS point densities calculated for SUs separately for ascending (a and c) and descending (b and d) orbits, respectively. The numbers indicated within circles represent sub-catchment IDs. The results were generated for PS points after filtering out values between the median velocity and one standard deviation.

Up to this point, we assessed the deformation at PS points and over SUs. To complete our study, we further upscaled our analyses, this time examining six sub-catchments. These were obtained as the expert combination of the previous SUs into larger geographical entities (Figs. 8c-8d, 9a and 10a). We did so to offer a different perspective of the deformation patterns and their temporal evolution, based on three simple sectors along the topographic profile: upper, middle and lower hillslopes. Specifically, we used the six sub-catchments to cluster PS points selecting downslope velocities within the inter-quartile range of the whole distribution. We then compared high deformation zones in both ascending and descending orbits.

Figures 8c and 8d summarize downslope velocities aggregated for the sub-catchments. At the lower part of the examined hillslope (i.e., Sub-catchments 4 and 5), mean downslope velocities are quite similar in both orbits and ranging between 23 and 35 mm/year. In the middle part (i.e., Sub-catchments 2 and 3) the difference is higher and reach up to 10-15 mm/year. At the upper part (Sub-catchment 1), the difference in mean velocity is around 25 mm/year. We observed the highest difference in Sub-catchment 6 where PS density is quite low in both cases (Fig. 8).

Figures 9a and 10a provided another clear indication that the area is slowly moving. Similar to Figure 8, we filtered out all the velocities outside the interquartile range. The vast majority of the remaining PS points all fell within the examined watershed, in the case of both orbits. In particular, they concentrated within Sub-catchments 1, 2, 3 and 5 (Figs. 9a and 10a).

The downslope deformation time-series presented a continuous deformation, but each time-series is interrupted by some noticeable short-term fluctuations (Figs. 9 and 10), in both orbits. To explore the causes behind these fluctuations, we accessed and overlaid temperature and fraction of snow cover for each sub-catchment onto the velocity data. Results showed a clear link between these and specifically with respect to the snow cover time-series. Specifically, the snow cover is generally present from mid-November to mid-March, which is likely responsible for the fluctuation in the SAR signals. Nevertheless, even when excluding the noisy signal due to snow, the overall trend still indicates a clear and continuous deformation.

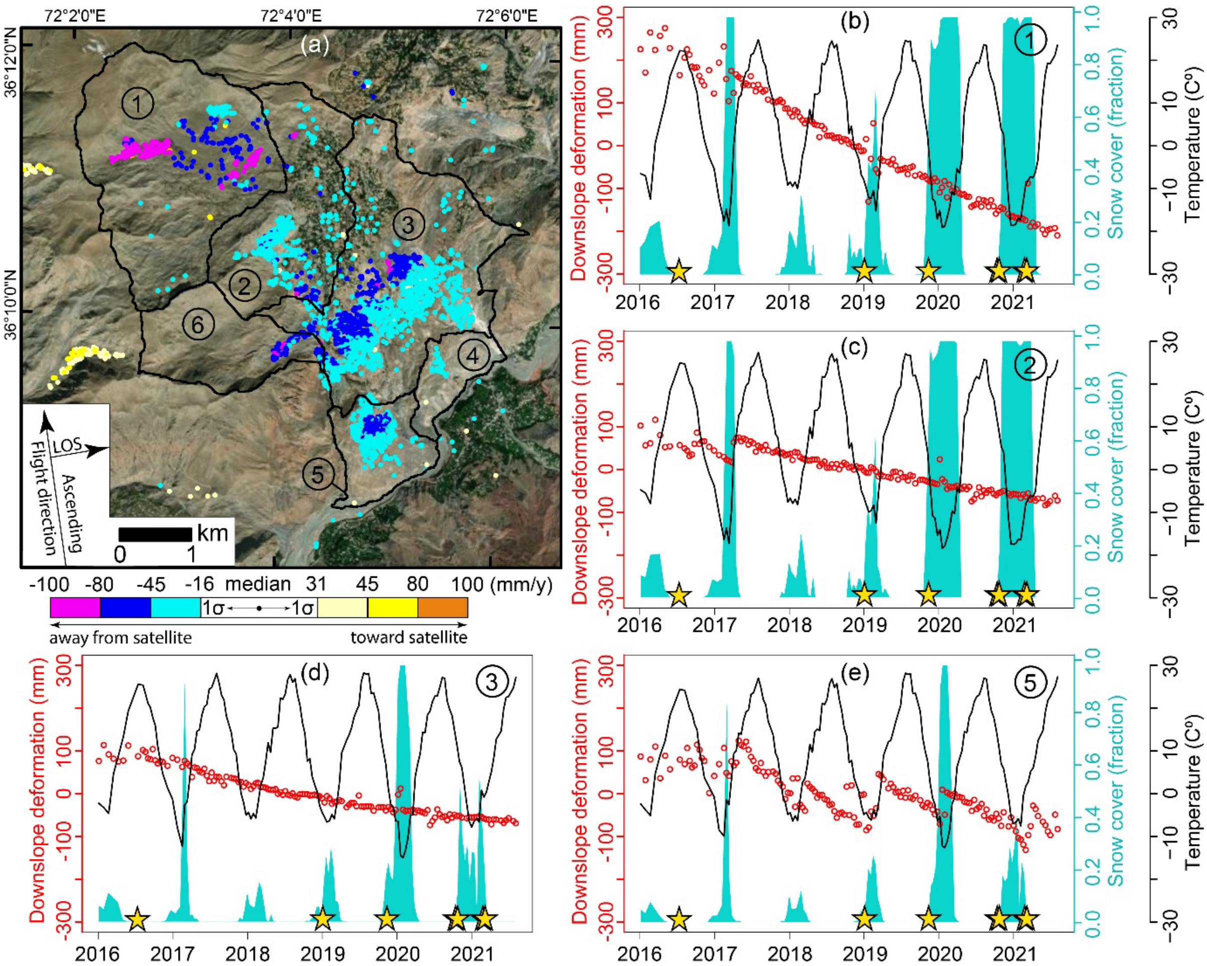

Figure 9. Average downslope velocities in ascending orbit overlaid by aggregated SUs representing sub-catchments of the study area (a) and average downslope time series generated for each sub-catchment overlaid by both fraction of snow cover and temperature (b-d). Yellow stars indicate date of earthquakes ($M_w \geq 4.0$) occurred in the vicinity (i.e., distance to source<60km). The numbers indicated within circles represent sub-catchment IDs.

Aside from the fluctuations, a signal that cannot be justified just through noise stands out in the deformation captured through the ascending orbit. In Figure 9e, a systematic offset is shown to occur every spring, this time being completely uncorrelated to the snow cover signals. Conversely, this systematic offset matches the start of the warm season. This signal is only present in the ascending orbit at Sub-catchment 5, which corresponds to the toe of the old landslide. In the descending orbit same signal does not appear when we examine the average downslope time series for the entire Sub-catchment 5. However, we can still capture similar offset associated with individual PS points (Figs. 10f and 10g). Bringing all these pieces together, these offsets might be interpreted as the presence of relatively rapid deformations/failures occurring every spring.

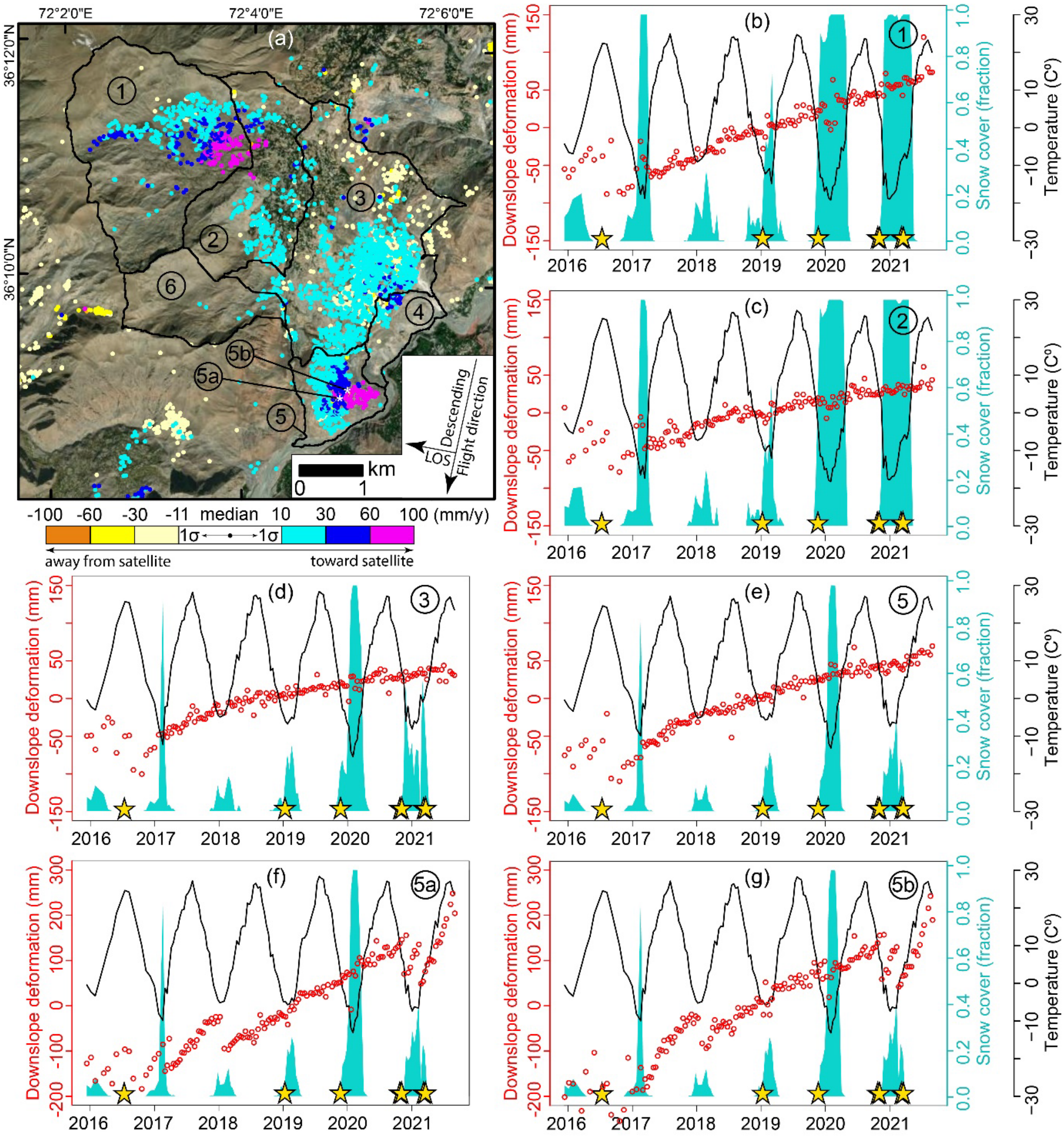

Figure 10. Average downslope velocities in descending orbit overlaid by aggregated SUs representing sub-catchments of the study area (a), average downslope time series generated for each sub-catchment (b-d) and two PS points from the lower part of the hillslope (f-g) overlaid by both fraction of snow cover and temperature (b-d). Yellow stars indicate the date of earthquakes ($M_w \geq 4.0$) occurred in the vicinity (i.e., distance to source<60km). The numbers indicated within circles represent sub-catchment IDs.

Other than climatic variables, we finally also checked the possible role of earthquakes on deformation time series. We did so by identifying earthquakes of magnitude greater than 4.0 that occurred in a zone 60 km distances from the study area. Figures 9 and 10 show the surface deformation time series overlaid by those earthquakes. However, no clear surface response was captured associated with given earthquakes.

5. Discussion

Monitoring hillslope deformations through satellite-based radar data can provide insightful observations of landscape responses to external stress sources. Freely available Sentinel-1 data allows InSAR time series analyses, especially in remote areas of low or medium-income countries. This can offer a unique opportunity to assess landslide susceptibility and hazard.

Landslide susceptibility is usually expressed via maps that indicate where landslides are probabilistically likely to occur. Hazard maps extend the definition accounting for when or how often (Guzzetti et al., 1999), as well as how many (Lombardo et al., 2018) or how large those landslides might be (Lombardo et al., 2021) or how fast they may travel (Corominas et al., 2014). Traditionally, landslide susceptibility and hazard maps are generated on the basis of either historical inventories or on the basis of event-based inventories. The latter encompass landslides that occur in response to a specific trigger such as rainfall, earthquake or snow melt. However, in an area dominated by large, slow-moving landslides, traditional methods may not be effective. For instance, the slow-moving landslide we examined in this study hosts/generates a number of relatively small, shallow, flow-type nested landslides. Mapping those small landslides via geomorphological mapping could be used to generate a susceptibility map. And yet, if the entire hillslope is moving downslope as we observed in our case, assessing the susceptibility of small landslides could underestimate a much larger threat posed by the slow-moving landslide body as a whole. Similarly, a landslide hazard map could be produced by identifying those small landslides with a proxy to their intensity level (e.g., landslide velocity or area). However, estimating the timing of those small landslides and their intensities would not reflect the overall hazard, for instance, the Loan and Reshun villages would be exposed to. Aside from these recent and shallow landslides, if we would focus on the main threat represented by the underlying large landslide body, even in this case a traditional susceptibility or hazard assessment will not provide much value. In fact, the susceptibility is obvious per se because the body slowly moves and the temporal definition of the hazard (i.e., how often/when) will be impossible to address because nobody, not even local inhabitants of the villages have memory of when the large failure occurred. Thus, a modern hazard assessment framework is required in such situations. This is of particular importance across the HHK mountain range, where snow cover is rapidly thawing. This effect may lubricate the sliding surfaces of former dormant landslides and lead to catastrophic consequences. Therefore, the possible link between climate change and landsliding requires special attention to holistically assess landslide susceptibility, hazard and risk.

The modern hazard assessment we mentioned above can come through the application of InSAR analyses, and this is also the approach we chose in this work. Specifically, our results provide insight into the dynamics of the slow-moving landslide threatening both the Loan and Reshun villages. The InSAR-based deformation time series we generated confirmed the continuous downslope motion in the last six years. This observation both applies to the ascending and descending orbits. Another relevant observation consists in the overall trend the time series present. In both orbits, Sub-catchment 1 highlights a worrisome linear pattern associated with the largest deformation of the whole hillslope (See Figs. 9b and 10b). This could be due to its relatively steep topography (see Fig. 5). Conversely, the deformation trend is more gentle in Sub-catchments 2 and 4. Figs. 9d and Fig. 10c-d actually reflect a sort of stabilizing trend in the last two years. The same figures show that the lowest temperatures and fractions of snow covers indicate that, from 2020 to 2021, the study area experienced relatively colder winter and spring seasons. Therefore, the stabilizing trend observed in the last two years may be consistent with the recent thick presence of snow cover in the study area. In other words, more snow may indicate, more albedo and thus less thawing.

The presence of radar visibility and sensitivity-related issues can hinder the clarity in the overall deformation mapped from both orbits. For instance, the deformation time series generated for the ascending orbit provides some signals which is not visible in the descending case. Figure 9 highlights that at toe of landslide zone, the radar data collected in the ascending direction captured some repeated deformation offsets occurring every spring. We interpreted them as a sign of relatively rapid deformations/failures. Such a signal can be only justified through the disturbance introduced by seasonally water discharges, mostly in the form of water influx from thawed snow cover. The resulting water can then infiltrate and act from the top as well as transform into runoff and increase the discharge of the Mastuj River and its capacity to incise the base of the slope. We thought that rainfall be responsible either for the entire or part of the deformation, rather than the water coming from the snow-covered ridges above the study area. We explore this assumption in Figure 11, using daily CHIRPS precipitation data (Funk et al., 2015). However, between the two possible sources of water in the system, the contribution of the rainfall seems minor. In fact, the maximum 12-day accumulated precipitation is around 60 mm at most for the whole examined period. As a result, we interpreted the snowmelt due to increasing temperatures to be the root cause of the “rapid” deformation we observed in spring.

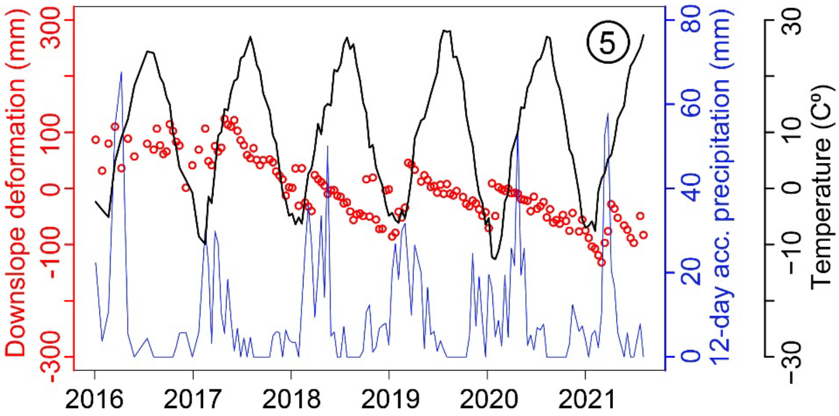

Figure 11. Figure showing the average downslope time series generated from ascending orbit for Sub-catchment 5 overlaid by both 12-day accumulated precipitation and temperature. For the precipitation, CHIRPS data (McNally, 2018) with 0.05° spatial resolution was used.

We maintain this interpretation for the deformation we observed at the foothill, as we excludes other geomorphologically-reasonable causes in the form of anthropogenic factors, earthquakes and/or tectonic uplifting. Anthropogenic influences are negligible, as the area is quite remote and has limited signs of significant man-made changes (e.g., road projects, terraces, dams, etc.). The local villages do not make use of irrigation, and depend on rainfed agriculture. Also, earthquakes would not be able to justify the overall deformation trend as no major earthquake occurred in the vicinity of the study area. At best, the seismic disturbance could represent a secondary factor in the form of legacy effect (Tanyaş et al., 2021). Similarly, tectonic uplifting of the entire area might only partially explain the evidence in surface deformation rates.

Under the assumption that the main phenomenon responsible for the deformation observed at the foothill of the study site is the snow melt, then it only makes sense to extend this interpretation to the whole catchment. If this interpretation is valid, then the contribution of snow melt to the instability of the study area needs to be further explored. We briefly introduced that we consider both infiltration and river incision to be the main drivers of the deformation.

The river incision is hydrologically plausible and the deformation record could confirm it to some extent. In fact, such incision leads to the development of relatively fast deformations or landslides and even up to the rock avalanches and debris slides we already showed in Figure 4f. Being the watershed approximately ~8 km long, then the relatively slower deformation rate we observe going uphill makes sense because the faster rates occur in the proximity to the channel and their effects slowly retrograde upward. However, this deformation model does not explain the extremely large deformation estimated at the top of the catchment. There, another process is required even beyond the intuitive role of the steep topography. Such a role can only be filled by the incoming water from further above. This water should be released from snow and thus could infiltrate and generate diffused instabilities. In light of this interpretation, we sought for signs of standing water or any other manifestation such as natural springs. During the interviews, villagers pointed out at a series of locations where they reported such springs to be quite diffused, specifically mentioning their seasonal appearance right after spring. Figure 12 shows the locations they indicated. Panel a highlights the presence of snow cover as well as the artificial water channels the local ancestors excavated to make use of the natural springtime runoff. As for panel b, there we show the water seepage we found along the upper part of the hillslope. Notably, this picture was captured during autumn. Thus, the discharge of these springs could only be much worse during the warmer seasons. Interestingly, both scenes offer a unique perspective to at least date the large landslide in recent times. In fact, the previous channel dug by villagers is suddenly interrupted by the line delimiting the landslide crown. We can safely assume that the failure occurred after the trench was made. Local villagers do not use these channels anymore to collect water. Thus, they could not provide any additional information that could be used to shed light on the role of those wet areas with respect to the continuous slope deformations we observed. Nevertheless, these incisions still exist and drain the incoming water along preferential directions.

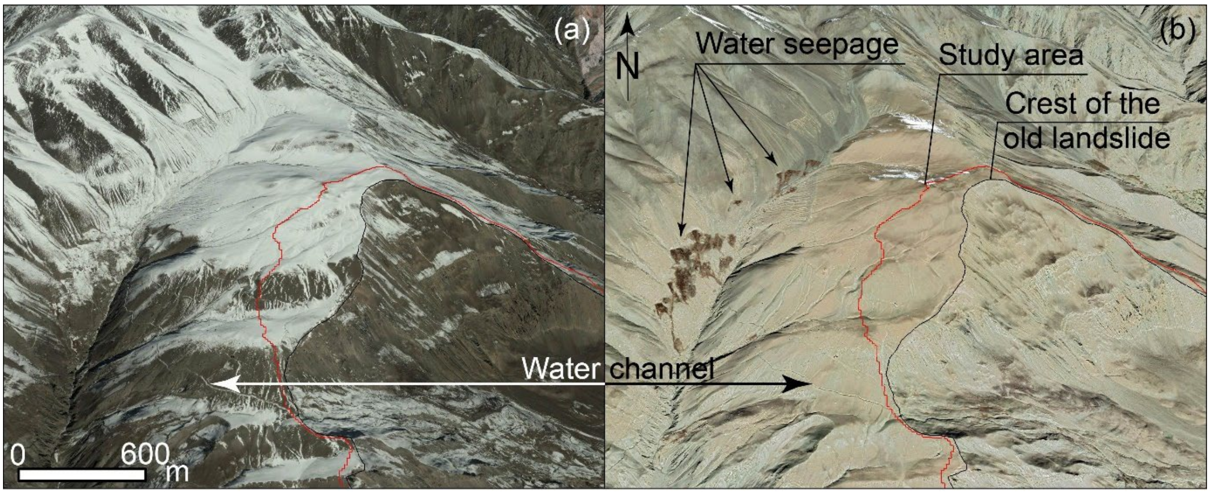

Figure 12. Google Earth scenes acquired on 12th of January 2018 (a) and 30th of October 2020 (b) showing snow cover and water seepage associated with thawing of snow cover as well as old water channels to provide the water requirements of nearby villages.

Before concluding, we would like to share another element of particular relevance, especially because we consider it a realistic risk for both villages, Loan standing on top of the large landslide itself and Reshun sitting at the bottom.

As briefly introduced in Section 2, we initially hypothesized that the old landslide was triggered by the failure of a part of the quartzite "wall" located at the toe of the hillslope (Fig. 3c). This crystalline barrier contributed by limiting any movement pushing from above; as it collapsed, so did the whole slope. Coming back to the present day, a portion of the original "wall" adjacent to the failed quartzite segment is still standing and may still provide the same stabilizing effect. However, if the "past is the key to the future" principle applies even under current conditions, the remaining quartzite barrier may also fail. In this case, the lives of the inhabitants of the two neighboring villages may be lost in such a catastrophic scenario. Unfortunately, radar visibility of this particular section of the slope was not particularly suitable (Fig. 6b). As a result, it was illuminated within a narrow radar swath, which in turn may not provide a conclusive description of the deformation in Sub-catchment 5 (see Figs. 10a and 10f). Nevertheless, even with the limited number of PS points available, we tried to generate the same type of summary plot as in the previous figures. The resulting patterns are shown in Figure 13a, where the near vertical transition from one village to another appears to be characterized by a number of shallow failures. As for the boundary of Sub-catchment 4, the PS points there do not provide enough information in the ascending orbit (Fig. 13b). However, this is not the case in descending orbit (Fig. 13c), where three trends in the time series can be roughly discerned. These indicate some worrying signals of potential instability. In fact, recent periods (i.e., 2020 onwards) have shown a slight increase in the downslope deformation rate. Such observation also needs to be put into context. The large mass moving behind this quartzite block returned slightly lower downslope deformation values right at the boundary with Sub-catchment 4 over the six years under examination. Below, the quartzite block overlooking Reshun is characterized by slightly faster deformation rates. This could indicate the accumulation of stress and a resulting strain release of the quartzite block itself. This in time could further destabilize into a paroxysmal release. Signs of such potential destabilizations should consist in deformation rates that exhibit some degree of acceleration in time, which at least in part is what we see in Figure 13c.

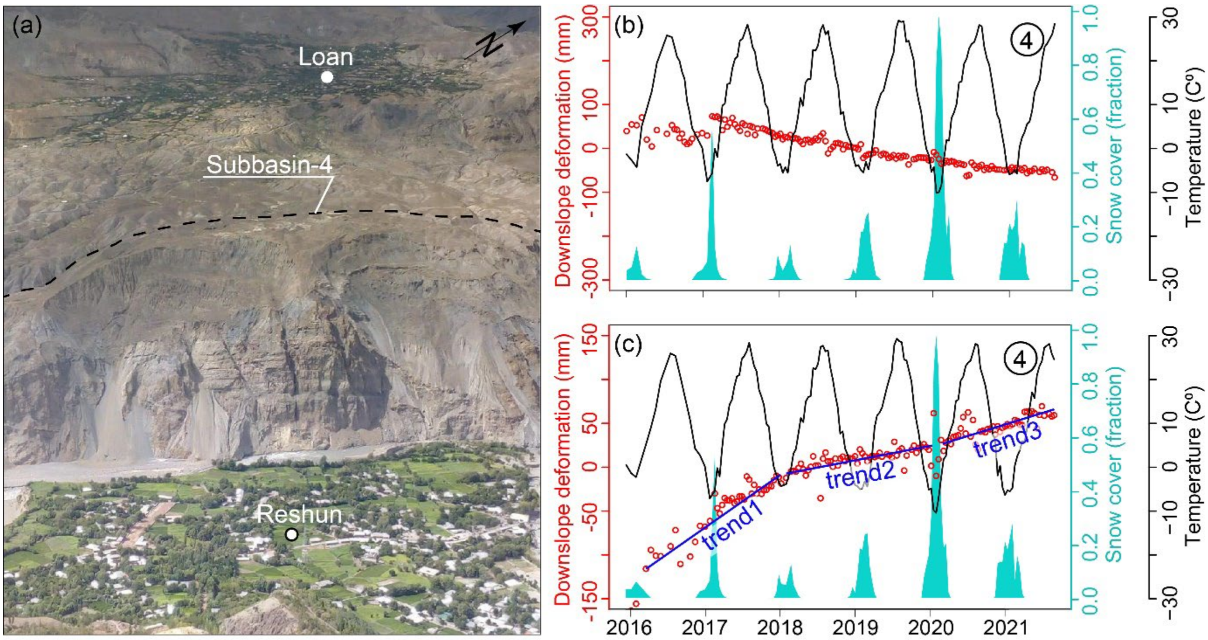

Figure 13. (a) View of the quartzite "wall" which separates the moving body where the village of Loan is located and the floodplain where the village of Reshun has been built. (b) and (c) are the time series of downslope deformation plotted together with snow cover and temperature data, in their respective ascending and descending orbits.

6. Conclusions

InSAR time series analysis techniques have been successfully employed for monitoring slow-moving landslides over the last decade. We chose their use in the context of this study area because of the slope's complexity, and the risk to the two villages. Our interpretation is that the melting process of snow cover from the higher portions of the relief contributes to a large rock slide and a number of smaller failures along this huge body. The thawing could be potentially linked to climate change because the temperature in Hindukush-Himalayan range has rapidly increased in recent years. The radar scenes we examined only go back six years ago. However, this data is already sufficient to at least depict a scenario that calls for further studies, if not more drastic actions. The moving body can be visualized in sections along the topographic profile, the highest being also the most dynamic one. Then, the central portion is characterized by slower movements. And, the lowest sector is divided into two sub-areas. A western one, where the former quartzite barrier might have already collapsed. There, the deformation is faster and the material slowly moves with sudden episodes of acceleration during spring. These are likely due to the contextual action of the basal stream erosion as well as the lubrication coming from infiltrated water of the melting snow cover. This already represents a worrying situation, but to some extent the material is sliding downhill, allowing the whole body to release the accumulated friction. However, this is not the case in the eastern area of the lowest sector. There, the quartzite barrier constantly shows signs of instability, releasing shallow avalanches and debris slides over the “cliff” face. And, most importantly, it shows accelerated trends of deformation along the crown (or what we called the boundary of Sub-catchment 4). This may end up in a paroxysmal failure in the same way it occurred right next to it in the past. If so, then the two villages of Loan and Reshun may be involved in a catastrophe. We are already in contact with Pakistani colleagues and have shared this observation beyond the scope of this research, with the intent of at least raising awareness and putting into place additional monitoring systems and potentially adequate plans to address the situation.

Going back to the more scientific aspect of this research, such a detailed description would not have been possible with other traditional means of geomorphological investigation. This is why we stress once more that use of InSAR is an important tool for hazard assessment and why we consider its implementation a valuable source of information to unveil the potential link between climate change and landscape evolution processes.

Acknowledgements

We are very grateful to Fazle Yar Khan for assisting us during field visits and providing us with valuable information regarding surface deformation experienced by local people.

Author contribution:

- HT devised the research idea.
- NS, SMA, MKE, IF, AA and HT performed the analyses
- HT and LL wrote the manuscript
- CJVW provided feedback on the manuscript
- ML is the institutional supervision of SMA

References

Al-Umar, M., Fall, M., Daneshfar, B., 2020. GIS-based modeling of snowmelt-induced landslide susceptibility of sensitive marine clays. Geoenvironmental Disasters 7. https://doi.org/10.1186/s40677-020-0142-8

Alvioli, M., Marchesini, I., Reichenbach, P., Rossi, M., Ardizzone, F., Fiorucci, F., Guzzetti, F., 2016. Automatic delineation of geomorphological slope units with r.slopeunits v1.0 and their optimization for landslide susceptibility modeling. Geosci. Model Dev. 9, 3975–3991. https://doi.org/10.5194/gmd-9-3975-2016

Ashish et al., 2006. No Title. Nat. Sci. 4, 53–95.

Aslan, G., Foumelis, M., Raucoules, D., De Michele, M., Bernardie, S., Cakir, Z., 2020. Landslide Mapping and Monitoring Using Persistent Scatterer Interferometry (PSI) Technique in the French Alps. Remote Sens. . https://doi.org/10.3390/rs12081305

Atta-ur-Rahman, Khan, A.N., Collins, A.E., Qazi, F., 2011. Causes and extent of environmental impacts of landslide hazard in the Himalayan region: a case study of Murree, Pakistan. Nat. Hazards 57, 413–434. https://doi.org/10.1007/s11069-010-9621-7

Bayer, B., Simoni, A., Mulas, M., Corsini, A., Schmidt, D., 2018. Deformation responses of slow moving landslides to seasonal rainfall in the Northern Apennines, measured by InSAR. Geomorphology 308, 293–306. https://doi.org/10.1016/j.geomorph.2018.02.020

Bekaert, D.P.S., Handwerger, A.L., Agram, P., Kirschbaum, D.B., 2020. InSAR-based detection method for mapping and monitoring slow-moving landslides in remote regions with steep and mountainous terrain: An application to Nepal. Remote Sens. Environ. 249, 111983. https://doi.org/https://doi.org/10.1016/j.rse.2020.111983

Beniston, M., Farinotti, D., Stoffel, M., Andreassen, L.M., Coppola, E., Eckert, N., Fantini, A., Giacona, F., Hauck, C., Huss, M., Huwald, H., Lehning, M., López-Moreno, J.I., Magnusson, J., Marty, C., Morán-Tejéda, E., Morin, S., Naaim, M., Provenzale, A., Rabatel, A., Six, D., Stötter, J., Strasser, U., Terzago, S., Vincent, C., 2018. The European mountain cryosphere: A review of its current state, trends, and future challenges. Cryosphere 12, 759–794. https://doi.org/10.5194/tc-12-759-2018

Bolch, T., Shea, J.M., Liu, S., Azam, F.M., Gao, Y., Gruber, S., Immerzeel, W.W., Kulkarni, A., Li, H., Tahir, A.A., Zhang, G., Zhang, Y., 2019. Status and Change of the Cryosphere in the Extended Hindu Kush Himalaya Region BT - The Hindu Kush Himalaya Assessment: Mountains, Climate Change, Sustainability and People, in: Wester, P., Mishra, A., Mukherji, A., Shrestha, A.B. (Eds.), . Springer International Publishing, Cham, pp. 209–255. https://doi.org/10.1007/978-3-319-92288-1_7

Bräuning, A., 2006. Tree-ring evidence of ‘Little Ice Age’ glacier advances in southern Tibet. The Holocene 16, 369–380. https://doi.org/10.1191/0959683606hl922rp

Carlà, T., Tofani, V., Lombardi, L., Raspini, F., Bianchini, S., Bertolo, D., Thuegaz, P., Casagli, N., 2019. Combination of GNSS, satellite InSAR, and GBInSAR remote sensing monitoring to improve the understanding of a large landslide in high alpine

environment. Geomorphology 335, 62–75. https://doi.org/https://doi.org/10.1016/j.geomorph.2019.03.014
Carrara, A., 1988. Drainage and divide networks derived from high-fidelity digital terrain models, in: Quantitative Analysis of Mineral and Energy Resources. Springer, pp. 581–597.
Casagli, N., Catani, F., Del Ventisette, C., Luzi, G., 2010. Monitoring, prediction, and early warning using ground-based radar interferometry. Landslides 7, 291–301.
Cascini, L., Fornaro, G., Peduto, D., 2010. Advanced low- and full-resolution DInSAR map generation for slow-moving landslide analysis at different scales. Eng. Geol. 112, 29–42. https://doi.org/https://doi.org/10.1016/j.enggeo.2010.01.003
Cigna, F., Bateson, L.B., Jordan, C.J., Dashwood, C., 2014. Simulating SAR geometric distortions and predicting Persistent Scatterer densities for ERS-1/2 and ENVISAT C-band SAR and InSAR applications: Nationwide feasibility assessment to monitor the landmass of Great Britain with SAR imagery. Remote Sens. Environ. 152, 441–466. https://doi.org/https://doi.org/10.1016/j.rse.2014.06.025
Colesanti, C., Wasowski, J., 2006. Investigating landslides with space-borne Synthetic Aperture Radar (SAR) interferometry. Eng. Geol. 88, 173–199. https://doi.org/https://doi.org/10.1016/j.enggeo.2006.09.013
Cook, N., Butz, D., 2013. The Atta Abad landslide and everyday mobility in Gojal, Northern Pakistan. Mt. Res. Dev. 33, 372–380. https://doi.org/10.1659/MRD-JOURNAL-D-13-00013.1
Corominas, J., van Westen, C., Frattini, P., Cascini, L., Malet, J.P., Fotopoulou, S., Catani, F., Van Den Eeckhaut, M., Mavrouli, O., Agliardi, F., Pitilakis, K., Winter, M.G., Pastor, M., Ferlisi, S., Tofani, V., Hervás, J., Smith, J.T., 2014. Recommendations for the quantitative analysis of landslide risk. Bull. Eng. Geol. Environ. 73, 209–263. https://doi.org/10.1007/s10064-013-0538-8
Coward, M.P., Rex, D.C., Asif Khan, M., Windley, B.F., Broughton, R.D., Luff, I.W., Petterson, M.G., Pudsey, C.J., 1986. Collision tectonics in the NW Himalayas. Geol. Soc. Spec. Publ. 19, 203–219. https://doi.org/10.1144/GSL.SP.1986.019.01.11
Dehn, M., Bürger, G., Buma, J., Gasparetto, P., 2000. Impact of climate change on slope stability using expanded downscaling. Eng. Geol. 55, 193–204. https://doi.org/10.1016/S0013-7952(99)00123-4
Eberhardt, E., Thuro, K., Luginbuehl, M., 2005. Slope instability mechanisms in dipping interbedded conglomerates and weathered marls - The 1999 Rufi landslide, Switzerland. Eng. Geol. 77, 35–56. https://doi.org/10.1016/j.enggeo.2004.08.004
Funk, C., Peterson, P., Landsfeld, M., Pedreros, D., Verdin, J., Shukla, S., Husak, G., Rowland, J., Harrison, L., Hoell, A., Michaelsen, J., 2015. The climate hazards infrared precipitation with stations—a new environmental record for monitoring extremes. Sci. Data 2, 150066. https://doi.org/10.1038/sdata.2015.66
Gaetani, M., Le Fort, P., Tanoli, S., Angiolini, L., Nicora, A., Sciunnach, D., Khan, A., 1996. Reconnaissance geology in Upper Chitral, Baroghil and Karambar districts (northern Karakorum, Pakistan). Int. J. Earth Sci. 85, 683–704. https://doi.org/10.1007/s005310050106
Gao, Y., Liu, S., Qi, M., Xie, F., Wu, K., Zhu, Y., 2021. Glacier-Related Hazards Along the International Karakoram Highway: Status and Future Perspectives. Front. Earth Sci. 9, 1–14. https://doi.org/10.3389/feart.2021.611501
Gariano, S.L., Guzzetti, F., 2016. Landslides in a changing climate. Earth-Science Rev. 162, 227–252. https://doi.org/https://doi.org/10.1016/j.earscirev.2016.08.011
Gerrard, J., 1994. The landslide hazard in the Himalayas: geological control and human action. Geomorphology 10, 221–230. https://doi.org/10.1016/0169-555X(94)90018-3
Gobiet, A., Kotlarski, S., 2020. Future Climate Change in the European Alps. https://doi.org/10.1093/acrefore/9780190228620.013.767
Gobiet, A., Kotlarski, S., Beniston, M., Heinrich, G., Rajczak, J., Stoffel, M., 2014. 21st century climate change in the European Alps-A review. Sci. Total Environ. 493, 1138–1151. https://doi.org/10.1016/j.scitotenv.2013.07.050

Gruber, S., Fleiner, R., Guegan, E., Panday, P., Schmid, M.-O., Stumm, D., Wester, P., Zhang, Y., Zhao, L., 2017. Review article: Inferring permafrost and permafrost thaw in the mountains of the Hindu Kush Himalaya region. Cryosph. 11, 81–99. https://doi.org/10.5194/tc-11-81-2017

Gruber, S., Haeberli, W., 2007. Permafrost in steep bedrock slopes and its temperatures-related destabilization following climate change. J. Geophys. Res. Earth Surf. 112, 1–10. https://doi.org/10.1029/2006JF000547

Gullà, G., Aceto, L., Antronico, L., Cilento, M., Niceforo, D., Perna, E., Terranova, O., 2004. Failure and post failure conditions of a landslide involving weathered and degraded rocks. Landslides Eval. Stab. Terrain Eval. Stabilisation, Set 2 Vol. 1240–1245. https://doi.org/10.1201/b16816-180

Guzzetti, F., Carrara, A., Cardinali, M., Reichenbach, P., 1999. Landslide hazard evaluation: a review of current techniques and their application in a multi-scale study, Central Italy. Geomorphology 31, 181–216. https://doi.org/https://doi.org/10.1016/S0169-555X(99)00078-1

Heuberger, S., Schaltegger, U., Burg, J.P., Villa, I.M., Frank, M., Dawood, H., Hussain, S., Zanchi, A., 2007. Age and isotopic constraints on magmatism along the Karakoram-Kohistan Suture Zone, NW Pakistan: Evidence for subduction and continued convergence after India-Asia collision. Swiss J. Geosci. 100, 85–107. https://doi.org/10.1007/s00015-007-1203-7

Hewitt, K., 2001. Catastrophic Rockslides and the Geomorphology of the Hunza and Gilgit River Valleys, Karakoram Himalaya (Katastrophale Bergstürze und die Geomorphologie der Hunza und Gilgit Flusstäler, Karakorum Himalaja). Erdkunde 55, 72–93.

Hewitt, K., Clague, J.J., Orwin, J.F., 2008. Legacies of catastrophic rock slope failures in mountain landscapes. Earth-Science Rev. 87, 1–38. https://doi.org/10.1016/j.earscirev.2007.10.002

Hilley, E.G., Roland, B., Alessandro, F., Fabrizio, N., Fabio, R., 2004. Dynamics of Slow-Moving Landslides from Permanent Scatterer Analysis. Science (80-.). 304, 1952–1955. https://doi.org/10.1126/science.1098821

Hooper, A., Bekaert, D., Spaans, K., Arikan, M., 2012. Recent advances in SAR interferometry time series analysis for measuring crustal deformation. Tectonophysics 514–517, 1–13. https://doi.org/10.1016/j.tecto.2011.10.013

Hooper, A.J., 2008. A multi-temporal InSAR method incorporating both persistent scatterer and small baseline approaches. Geophys. Res. Lett. 35, 1–5. https://doi.org/10.1029/2008GL034654

Huang Lin, C., Liu, D., Liu, G., 2019. Landslide detection in La Paz City (Bolivia) based on time series analysis of InSAR data. Int. J. Remote Sens. 40, 6775–6795. https://doi.org/10.1080/01431161.2019.1594434

Huffman, G., Stocker, E.F., T, B.D., Nelkin, E.J., Tan, J., 2019. GPM IMERG Final Precipitation L3 1 day 0.1 degree x 0.1 degree V06 [WWW Document]. Ed. by Andrey Savtchenko, Greenbelt, MD, Goddard Earth Sci. Data Inf. Serv. Cent. (GES DISC). https://doi.org/10.5067/GPM/IMERGDF/DAY/06

Huggel, C., Clague, J.J., Korup, O., 2012. Is climate change responsible for changing landslide activity in high mountains? Earth Surf. Process. Landforms 37, 77–91. https://doi.org/10.1002/esp.2223

Hungr, O., Evans, S.G., Bovis, M.J., Hutchinson, J.N., 2001. A review of the classification of landslides of the flow type. Environ. Eng. Geosci. 7, 221–238. https://doi.org/10.2113/gseegeosci.7.3.221

Huss, M., Hock, R., 2018. Global-scale hydrological response to future glacier mass loss. Nat. Clim. Chang. 8, 135–140. https://doi.org/10.1038/s41558-017-0049-x

Hussain, S., Hongxing, S., Ali, M., Sajjad, M.M., Afzal, Z., Ali, S., 2021. Optimized landslide susceptibility mapping and modelling using PS-InSAR technique: a case study of Chitral valley, Northern Pakistan. Geocarto Int. 0, 1–22. https://doi.org/10.1080/10106049.2021.1914750

Ikeda, K., Rasmussen, R., Liu, C., Newman, A., Chen, F., Barlage, M., Gutmann, E., Dudhia,

J., Dai, A., Luce, C., Musselman, K., 2021. Snowfall and snowpack in the Western U.S. as captured by convection permitting climate simulations: current climate and pseudo global warming future climate. Clim. Dyn. 57, 2191–2215. https://doi.org/10.1007/s00382-021-05805-w
IPCC, 2021. Summary for Policymakers. In: Climate Change 2021: The Physical Science Basis. Contribution of Working Group I to the Sixth Assessment Report of the Intergovernmental Panel on Climate Change [Masson-Delmotte, V., P. Zhai, A. Pirani, S. L. Connors, C. Péan.
Ishikawa, T., Tokoro, T., Seiichi, M., 2015. Geohazard at volcanic soil slope in cold regions and its influencing factors. Japanese Geotech. Soc. Spec. Publ. 1, 1–20. https://doi.org/10.3208/jgssp.key-1
Kargel, J.S., Leonard, G., Crippen, R.E., Delaney, K.B., Evans, S.G., Schneider, J., 2010. Satellite Monitoring of Pakistan's Rockslide-Dammed Lake Gojal. Eos, Trans. Am. Geophys. Union 91, 394–395. https://doi.org/10.1029/2010eo430002
Lacroix, P., Handwerger, A.L., Bièvre, G., 2020. Life and death of slow-moving landslides. Nat. Rev. Earth Environ. 1, 404–419. https://doi.org/10.1038/s43017-020-0072-8
Liu, X., Zhao, C., Zhang, Q., Lu, Z., Li, Z., Yang, C., Zhu, W., Liu-Zeng, J., Chen, L., Liu, C., 2021. Integration of Sentinel-1 and ALOS/PALSAR-2 SAR datasets for mapping active landslides along the Jinsha River corridor, China. Eng. Geol. 284, 106033. https://doi.org/https://doi.org/10.1016/j.enggeo.2021.106033
Loche, M., Scaringi, G., Yunus, A.P., Catani, F., Tanyaş, H., Frodella, W., Fan, X., Lombardo, L., 2022. Surface temperature controls the pattern of post-earthquake landslide activity. Sci. Rep. 12, 988. https://doi.org/10.1038/s41598-022-04992-8
Lombardo, L., Opitz, T., Huser, R., 2018. Point process-based modeling of multiple debris flow landslides using INLA: an application to the 2009 Messina disaster. Stoch. Environ. Res. Risk Assess. 32, 2179–2198. https://doi.org/10.1007/s00477-018-1518-0
Lombardo, L., Tanyas, H., Huser, R., Guzzetti, F., Castro-Camilo, D., 2021. Landslide size matters: A new data-driven, spatial prototype. Eng. Geol. 293, 106288. https://doi.org/https://doi.org/10.1016/j.enggeo.2021.106288
Marcer, M., Cicoira, A., Cusicanqui, D., Bodin, X., Echelard, T., Obregon, R., Schoeneich, P., 2021. Rock glaciers throughout the French Alps accelerated and destabilised since 1990 as air temperatures increased. Commun. Earth Environ. 2, 81. https://doi.org/10.1038/s43247-021-00150-6
Mccoll, S.T., Davies, T.R.H., 2013. Large ice-contact slope movements: Glacial buttressing, deformation and erosion. Earth Surf. Process. Landforms 38, 1102–1115. https://doi.org/10.1002/esp.3346
McNally, A., 2018. FLDAS Noah Land Surface Model L4 Global Monthly 0.1 x 0.1 degree (MERRA-2 and CHIRPS), Greenbelt, MD, USA, Goddard Earth Sciences Data and Information Services Center (GES DISC). https://doi.org/https://doi.org/10.5067/5NHC22T9375G
Mondini, A.C., Guzzetti, F., Chang, K.-T., Monserrat, O., Martha, T.R., Manconi, A., 2021. Landslide failures detection and mapping using Synthetic Aperture Radar: Past, present and future. Earth-Science Rev. 216, 103574. https://doi.org/https://doi.org/10.1016/j.earscirev.2021.103574
NASA JPL, 2013. NASA Shuttle Radar Topography Mission United States 1 Arc Second. NASA EOSDIS Land Processes DAAC, USGS Earth Resources Observation and Science (EROS) Center, Sioux Falls, South Dakota https://lpdaac.usgs.gov, Accessed date: 1 December 2019. [WWW Document].
Notti, D., Herrera, G., Bianchini, S., Meisina, C., García-Davalillo, J.C., Zucca, F., 2014. A methodology for improving landslide PSI data analysis. Int. J. Remote Sens. 35, 2186–2214. https://doi.org/10.1080/01431161.2014.889864
Osawa, H., Matsuura, S., Matsushi, Y., Okamoto, T., 2017. Seasonal change in permeability of surface soils on a slow-moving landslide in a heavy snow region. Eng. Geol. 221, 1–9. https://doi.org/10.1016/j.enggeo.2017.02.019
Pepin, N.C., Arnone, E., Gobiet, A., Haslinger, K., Kotlarski, S., Notarnicola, C., Palazzi, E.,

Seibert, P., Serafin, S., Schöner, W., Terzago, S., Thornton, J.M., Vuille, M., Adler, C., 2022. Climate Changes and Their Elevational Patterns in the Mountains of the World. Rev. Geophys. 60, e2020RG000730. https://doi.org/https://doi.org/10.1029/2020RG000730

Perissin, D., Wang, T., 2011. Time-Series InSAR Applications Over Urban Areas in China. IEEE J. Sel. Top. Appl. Earth Obs. Remote Sens. 4, 92–100. https://doi.org/10.1109/JSTARS.2010.2046883

Prasad, A.K., S. Yang, K.H., El-Askary, H.M., Kafatos, M., 2009. Melting of major Glaciers in the western Himalayas: Evidence of climatic changes from long term MSU derived tropospheric temperature trend (1979-2008). Ann. Geophys. 27, 4505–4519. https://doi.org/10.5194/angeo-27-4505-2009

Rahman, A. ur, Khan, A.N., Collins, A.E., 2014. Analysis of landslide causes and associated damages in the Kashmir Himalayas of Pakistan. Nat. Hazards 71, 803–821. https://doi.org/10.1007/s11069-013-0918-1

Ray, P.K.C., Parvaiz, I., Jayangondaperumal, R., Thakur, V.C., Dadhwal, V.K., Bhat, F.A., 2009. Analysis of seismicity-induced landslides due to the 8 October 2005 earthquake in Kashmir Himalaya. Curr. Sci. 97, 1742–1751.

Rehman, M.U., Zhang, Y., Meng, X., Su, X., Catani, F., Rehman, G., Yue, D., Khalid, Z., Ahmad, S., Ahmad, I., 2020. Analysis of Landslide Movements Using Interferometric Synthetic Aperture Radar: A Case Study in Hunza-Nagar Valley, Pakistan. Remote Sens. . https://doi.org/10.3390/rs12122054

Riaz, S., Wang, G., Basharat, M., Takara, K., 2019. Experimental investigation of a catastrophic landslide in northern Pakistan. Landslides 16, 2017–2032. https://doi.org/10.1007/s10346-019-01216-5

Samsonov, S., Dille, A., Dewitte, O., Kervyn, F., d'Oreye, N., 2020. Satellite interferometry for mapping surface deformation time series in one, two and three dimensions: A new method illustrated on a slow-moving landslide. Eng. Geol. 266, 105471. https://doi.org/https://doi.org/10.1016/j.enggeo.2019.105471

Sarwar, K., Rahman, M.U., 2016. Economic Impact of Mineral Resources : A Case Study of District 17, 54–60.

Sato, H.P., Une, H., 2016. Detection of the 2015 Gorkha earthquake-induced landslide surface deformation in Kathmandu using InSAR images from PALSAR-2 data. Earth, Planets Sp. 68, 47. https://doi.org/10.1186/s40623-016-0425-1

Schlögel, R., Doubre, C., Malet, J.-P., Masson, F., 2015. Landslide deformation monitoring with ALOS/PALSAR imagery: A D-InSAR geomorphological interpretation method. Geomorphology 231, 314–330. https://doi.org/https://doi.org/10.1016/j.geomorph.2014.11.031

Seneviratne, S.I., Nicholls, N., Easterling, D., Goodess, C.M., Kanae, S., Kossin, J., Luo, Y., Marengo, J., Mc Innes, K., Rahimi, M., Reichstein, M., Sorteberg, A., Vera, C., Zhang, X., Rusticucci, M., Semenov, V., Alexander, L. V., Allen, S., Benito, G., Cavazos, T., Clague, J., Conway, D., Della-Marta, P.M., Gerber, M., Gong, S., Goswami, B.N., Hemer, M., Huggel, C., Van den Hurk, B., Kharin, V. V., Kitoh, A., Klein Tank, A.M.G., Li, G., Mason, S., Mc Guire, W., Van Oldenborgh, G.J., Orlowsky, B., Smith, S., Thiaw, W., Velegrakis, A., Yiou, P., Zhang, T., Zhou, T., Zwiers, F.W., 2012. Changes in climate extremes and their impacts on the natural physical environment. Manag. Risks Extrem. Events Disasters to Adv. Clim. Chang. Adapt. Spec. Rep. Intergov. Panel Clim. Chang. 9781107025, 109–230. https://doi.org/10.1017/CBO9781139177245.006

Shafique, M., van der Meijde, M., Khan, M.A., 2016. A review of the 2005 Kashmir earthquake-induced landslides; from a remote sensing prospective. J. Asian Earth Sci. 118, 68–80. https://doi.org/10.1016/j.jseaes.2016.01.002

Stauffer, K.W., 1975. Reconnaissance geology of the Central Mastuj Valley, Chitral State, Pakistan, Open-File Report. https://doi.org/10.3133/ofr75556

Stoffel, M., Huggel, C., 2012. Effects of climate change on mass movements in mountain environments. Prog. Phys. Geogr. 36, 421–439. https://doi.org/10.1177/0309133312441010

Stoffel, M., Tiranti, D., Huggel, C., 2014. Climate change impacts on mass movements — Case studies from the European Alps. Sci. Total Environ. 493, 1255–1266. https://doi.org/https://doi.org/10.1016/j.scitotenv.2014.02.102

Tahirkheli, T., Shah, M.T., Khan, M.A., Bilqees, R., 2012. Mineralogy and geochemistry of diorites and associated hydrothermal sulfide mineralization of Gawuch Formation in Drosh area, Chitral, northern Pakistan. J. Himal. Earth Sci. 45, 31–52.

Tantianuparp, P., Shi, X., Zhang, L., Balz, T., Liao, M., 2013. Characterization of landslide deformations in three Gorges area using multiple inSAR data stacks. Remote Sens. 5, 2704–2719. https://doi.org/10.3390/rs5062704

Tanyaş, H., Kirschbaum, D., Görüm, T., van Westen, C.J., Tang, C., Lombardo, L., 2021. A closer look at factors governing landslide recovery time in post-seismic periods. Geomorphology 391, 107912. https://doi.org/https://doi.org/10.1016/j.geomorph.2021.107912

Tanyaş, H., Rossi, M., Alvioli, M., van Westen, C.J., Marchesini, I., 2019. A global slope unit-based method for the near real-time prediction of earthquake-induced landslides. Geomorphology 327, 126–146. https://doi.org/10.1016/j.geomorph.2018.10.022

USGS, 2021. United States geological survey earthquake portal. Earthquake Hazards Program [WWW Document]. URL https://www.usgs.gov/%0Anatural-hazards/earthquake-hazards/earthquakes (accessed 4.27.21).

Wasowski, J., Bovenga, F., 2014. Investigating landslides and unstable slopes with satellite Multi Temporal Interferometry: Current issues and future perspectives. Eng. Geol. 174, 103–138. https://doi.org/10.1016/j.enggeo.2014.03.003

Wasowski, J., Pisano, L., 2020. Long-term InSAR, borehole inclinometer, and rainfall records provide insight into the mechanism and activity patterns of an extremely slow urbanized landslide. Landslides 17, 445–457. https://doi.org/10.1007/s10346-019-01276-7

Xu, Y., Schulz, W.H., Lu, Z., Kim, J., Baxstrom, K., 2021. Geologic controls of slow-moving landslides near the US West Coast. Landslides 18, 3353–3365. https://doi.org/10.1007/s10346-021-01732-3

Zanchi, A., Gaetani, M., 2011. The geology of the Karakoram range, Pakistan: The new 1:100,000 geological map of Central-Western Karakoram. Ital. J. Geosci. 130, 161–262. https://doi.org/10.3301/IJG.2011.09

Zanchi, A., Gaetani, M., Poli, S., 1997. The Rich Gol Metamorphic Complex: evidence of separation between Hindu Kush and Karakorum (Pakistan). Comptes Rendus l'Académie des Sci. - Ser. IIA - Earth Planet. Sci. 325, 877–882. https://doi.org/10.1016/s1251-8050(99)80188-8

Zemp, M., Huss, M., Thibert, E., Eckert, N., McNabb, R., Huber, J., Barandun, M., Machguth, H., Nussbaumer, S.U., Gärtner-Roer, I., Thomson, L., Paul, F., Maussion, F., Kutuzov, S., Cogley, J.G., 2019. Global glacier mass changes and their contributions to sea-level rise from 1961 to 2016. Nature 568, 382–386. https://doi.org/10.1038/s41586-019-1071-0

Zischinsky, U., 1968. Über Bergzerreißung und Talzuschub. Geol. Rundschau 58, 974–983. https://doi.org/10.1007/BF01820741